

The D^*/D ratio in heavy ion collisions

L. M. Abreu* and H. P. L. Vieira†
*Instituto de Física, Universidade Federal da Bahia,
Campus Universitário de Ondina, 40170-115, Bahia, Brazil*

F. S. Navarra‡
*Instituto de Física, Universidade de São Paulo,
Rua do Matão, 1371, CEP 05508-090,
São Paulo, SP, Brazil*

In this work we study the D^* and D multiplicities and how they change during the hadron gas phase of heavy ion collisions. With the help of an effective Lagrangian formalism, we calculate the production and absorption cross sections of the D^* and D mesons in a hadronic medium. We compute the time evolution of the abundances and the ratio D^*/D . They are approximately constant in time. Also, assuming a Bjorken type cooling and using an empirical relation between the freeze-out temperature and the central multiplicity density, we estimate D^*/D as a function of $dN/d\eta(\eta = 0)$, which represents the system size. We find that, while the number of D^* 's and D 's grows significantly with the system size, their ratio remains approximately constant. This prediction can be compared with future experimental data. Our results suggest that the charm meson interactions in the hadron gas do not change their multiplicities and consequently these mesons are close to chemical equilibrium.

I. INTRODUCTION

It is well accepted that nuclear matter at high temperatures or high densities experiences a phase transition to a deconfined phase of quarks and gluons, the so-called quark-gluon plasma (QGP), in which the fundamental degrees of freedom (quarks and gluons) behave as free particles [1–4]. This deconfined medium can be produced in heavy-ion collisions, where a hot and dense QGP fireball is created. This system expands and cools down as time evolves. At a certain point quarks, antiquarks and gluons recombine and form a hot hadron gas. The properties of this hot and dense system may be accessed through the study of observables, such as the hadron multiplicities.

As it has been often pointed out, heavy mesons are of great importance. They contain heavy quarks, which are produced in the early stages of the collision. They can carry unique information about the QGP, unlike light mesons that can be produced in the hadronic medium at later stages. However, charm mesons can be created and destroyed in collisions with the comoving mesons in the hadron gas. For this reason, the knowledge of the interactions of D^* and D mesons with light mesons is crucial for the calculation of the final abundances of such particles. With this motivation, the propagation of heavy-light mesons in a thermal medium has been intensively studied in different frameworks (we refer the reader to Ref. [5] for a review).

In the hadronic phase, the different species of hadrons undergo inelastic reactions, and their multiplicities can

be modified until the kinetic freeze-out, when there are no more interactions and the particles travel to reach the detectors. After hadronization and before the kinetic freeze-out, the hadron gas may be in a state where the production and absorption reactions occur with an equal rate and hence particle abundances do not change any more. This is called chemical equilibrium. In principle the emergence of chemical equilibrium could be studied numerically. Knowing the multiplicities of the particles of all species at the hadronization time and also knowing all their interaction cross sections, we could write and solve a set of coupled rate equations. We would then find the multiplicities as a function of time and we could determine the chemical freeze-out time (and the corresponding chemical freeze-out temperature), i.e., the time from which on all the multiplicities are frozen. Unfortunately, this calculation can not be done because we do not know all the required cross sections. However, we have now a reasonable knowledge of some subsets of the cross sections and we can find partial solutions for the general equilibration problem. We can, for example, determine what happens to K^* in the hadron gas phase, as it was done in [6]. Alternatively, we can postulate that chemical equilibrium is reached and use statistical mechanics to compute, in terms of a small number of parameters, the particle multiplicities, as it is done in the Statistical Hadronization Model (SHM) [7]. The success of the SHM in reproducing the observed multiplicities strongly suggests that hadron gas formed in heavy ion collisions is indeed in chemical equilibrium. However, this hypothesis, should at some point, be confirmed by microscopic calculations. In the charm sector, there has been a continuous progress in the study of the interaction cross sections of charm mesons. One of the goals of this work is to study the evolution of the D^* and D populations with a microscopic approach and check whether these mesons

* luciano.abreu@ufba.br

† hilde_son@hotmail.com

‡ navarra@if.usp.br

reach chemical equilibrium or not.

Recently, the production of prompt D^0 , D^+ and D^{*+} mesons at midrapidity ($|y| < 0.5$) in Pb–Pb collisions, at the centre-of-mass energy per nucleon–nucleon pair $\sqrt{s_{NN}} = 5.02$ TeV has been investigated by the ALICE collaboration [8]. Unfortunately, the system size (represented by $dN/d\eta(\eta = 0)$) dependence of the D^*/D ratio was not yet reported, as it was for strange mesons in [9]. This measurement is very interesting since different system sizes represent different samples of hadron gas with different lifetimes. Longer living systems are most likely to reach chemical equilibrium, whereas short living systems are less likely.

In a previous work, we have investigated the strange sector by evaluating the ratio between the K^* and K yields (K^*/K) as a function of the proper time, using the thermal cross sections of the interactions of the $K^{(*)}$ mesons with other light mesons as input in the rate equations [6]. The obtained ratio was in very good agreement with experimental data [9]. A similar analysis in the charm sector is going to be presented in what follows.

The purpose of this work is to extend the formalism used in [6] to evaluate the time evolution of the ratio D^*/D during the hadron gas phase of heavy ion collisions. We calculate the production and absorption cross sections of the D^* and D mesons with the help of an effective Lagrangian formalism, and use them in rate equations to compute the time evolution of the D^* and D abundances and the ratio D^*/D . Finally we estimate D^*/D as a function of the central multiplicity density ($dN/d\eta(\eta = 0)$).

The paper is organized as follows. In Section II we describe the effective formalism and introduce the thermally averaged cross sections of the $D^{(*)}$ -absorption and production reactions. In Section III we present and analyze the time evolution of the ratio D^*/D and its relation with the central multiplicity density. Finally, Section IV is devoted to the summary of the main points and to the concluding remarks. In Appendix the explicit expressions for the contributions to the amplitudes of the considered processes are given.

II. INTERACTIONS OF D AND D^* WITH LIGHT MESONS

A. Effective Lagrangians and reactions

In the present study, the reactions involving the interactions of D and D^* mesons with π and ρ mesons as well as between them will be analyzed within an effective field theory approach. In particular, we focus on the lowest-order Born contributions to the D^* and D absorption reactions shown in Figs. 1 and 2, as well as their inverse processes. To calculate their respective cross sections, we follow Refs. [6, 10, 11] and employ the effective

Lagrangians involving π , ρ , D and D^* mesons [12–17],

$$\begin{aligned}\mathcal{L}_{\pi DD^*} &= ig_{\pi DD^*} D^{*\mu} \vec{\tau} \cdot (\vec{D} \partial_\mu \vec{\pi} - \partial_\mu \vec{D} \vec{\pi}) + h.c., \\ \mathcal{L}_{\rho DD} &= ig_{\rho DD} (D \vec{\tau} \partial_\mu \vec{D} - \partial_\mu D \vec{\tau} \vec{D}) \cdot \vec{\rho}^\mu, \\ \mathcal{L}_{\rho D^* D^*} &= ig_{\rho D^* D^*} [(\partial_\mu D^{*\nu} \vec{\tau} \vec{D}_\nu^* - D^{*\nu} \vec{\tau} \partial_\mu \vec{D}_\nu^*) \cdot \vec{\rho}^\mu \\ &\quad + (D^{*\nu} \vec{\tau} \cdot \partial_\mu \vec{\rho}_\nu - \partial_\mu D^{*\nu} \vec{\tau} \cdot \vec{\rho}_\nu) \vec{D}^{*\mu} \\ &\quad + D^{*\mu} (\vec{\tau} \cdot \vec{\rho}^\nu \partial_\mu \vec{D}_\nu^* - \vec{\tau} \cdot \partial_\mu \vec{\rho}^\nu \vec{D}_\nu^*)], \\ \mathcal{L}_{\pi D^* D^*} &= -g_{\pi D^* D^*} \epsilon^{\mu\nu\alpha\beta} \partial_\mu D_\nu^* \pi \partial_\alpha \vec{D}_\beta^*, \\ \mathcal{L}_{\rho D D^*} &= -g_{\rho D D^*} \epsilon^{\mu\nu\alpha\beta} (D \partial_\mu \rho_\nu \partial_\alpha \vec{D}_\beta + \partial_\mu D \partial_\alpha \rho_\beta \vec{D})\end{aligned}\quad (1)$$

where $\vec{\tau}$ are the Pauli matrices in the isospin space; $\vec{\pi}$ denotes the pion isospin triplet; and $D^{(*)} = (D^{(*)0}, D^{(*)+})$ represents the isospin doublets for the pseudoscalar (vector) $D^{(*)}$ mesons. The coupling constants $g_{\pi DD^*}$, $g_{\rho DD}$, $g_{\rho D^* D^*}$, $g_{\pi D^* D^*}$ and $g_{\rho D D^*}$ will have their values given in the next section.

With the effective Lagrangians introduced above, the amplitudes of the D^* and D absorption processes shown in Figs. 1 and 2 can be calculated and are given by

$$\begin{aligned}\mathcal{M}_{D^* \pi \rightarrow \rho D} &= \mathcal{M}_{(1a)} + \mathcal{M}_{(1b)} + \mathcal{M}_{(1c)}, \\ \mathcal{M}_{D^* \rho \rightarrow \pi D} &= \mathcal{M}_{(2a)} + \mathcal{M}_{(2b)} + \mathcal{M}_{(2c)}, \\ \mathcal{M}_{D^* \bar{D} \rightarrow \rho \pi} &= \mathcal{M}_{(3a)} + \mathcal{M}_{(3b)} + \mathcal{M}_{(3c)}, \\ \mathcal{M}_{D^* \bar{D}^* \rightarrow \pi \pi} &= \mathcal{M}_{(4a)} + \mathcal{M}_{(4b)} + \mathcal{M}_{(4c)} + \mathcal{M}_{(4d)}, \\ \mathcal{M}_{D^* \bar{D}^* \rightarrow \rho \rho} &= \mathcal{M}_{(5a)} + \mathcal{M}_{(5b)} + \mathcal{M}_{(5c)} + \mathcal{M}_{(5d)}, \\ \mathcal{M}_{D \bar{D} \rightarrow \pi \pi} &= \mathcal{M}_{(6a)} + \mathcal{M}_{(6b)}, \\ \mathcal{M}_{D \bar{D} \rightarrow \rho \rho} &= \mathcal{M}_{(7a)} + \mathcal{M}_{(7b)} + \mathcal{M}_{(7c)} + \mathcal{M}_{(7d)},\end{aligned}\quad (2)$$

where the expressions for each contribution $\mathcal{M}_{(p)}$ are explicitly summarized in Appendix A. We mention that, in contrast to the works involving the strange mesons [6, 10, 11], here we do not consider the decay width Γ_{D^*} in the propagators of the intermediate vector charmed mesons, since it is very small and does not change our results significantly.

B. Cross sections

The isospin-spin-averaged cross section in the center of mass (CM) frame for the processes in Eq. (2) is given by:

$$\sigma_r^{(\varphi)}(s) = \frac{1}{64\pi^2 s} \frac{|\vec{p}_f|}{|\vec{p}_i|} \int d\Omega \overline{\sum_{S,I}} |\mathcal{M}_r^{(\varphi)}(s, \theta)|^2, \quad (3)$$

where r denominates the reactions according to Eq. (2); \sqrt{s} is the CM energy; $|\vec{p}_i|$ and $|\vec{p}_f|$ denote the three-momenta of initial and final particles in the CM frame, respectively; the symbol $\overline{\sum_{S,I}}$ stands for the sum over the spins and isospins of the particles in the initial and final state, weighted by the isospin and spin degeneracy factors of the two particles forming the initial state for the reaction r , i.e.

$$\overline{\sum_{S,I}} |\mathcal{M}_r|^2 \rightarrow \frac{1}{g_{1i,r}} \frac{1}{g_{2i,r}} \sum_{S,I} |\mathcal{M}_r|^2, \quad (4)$$

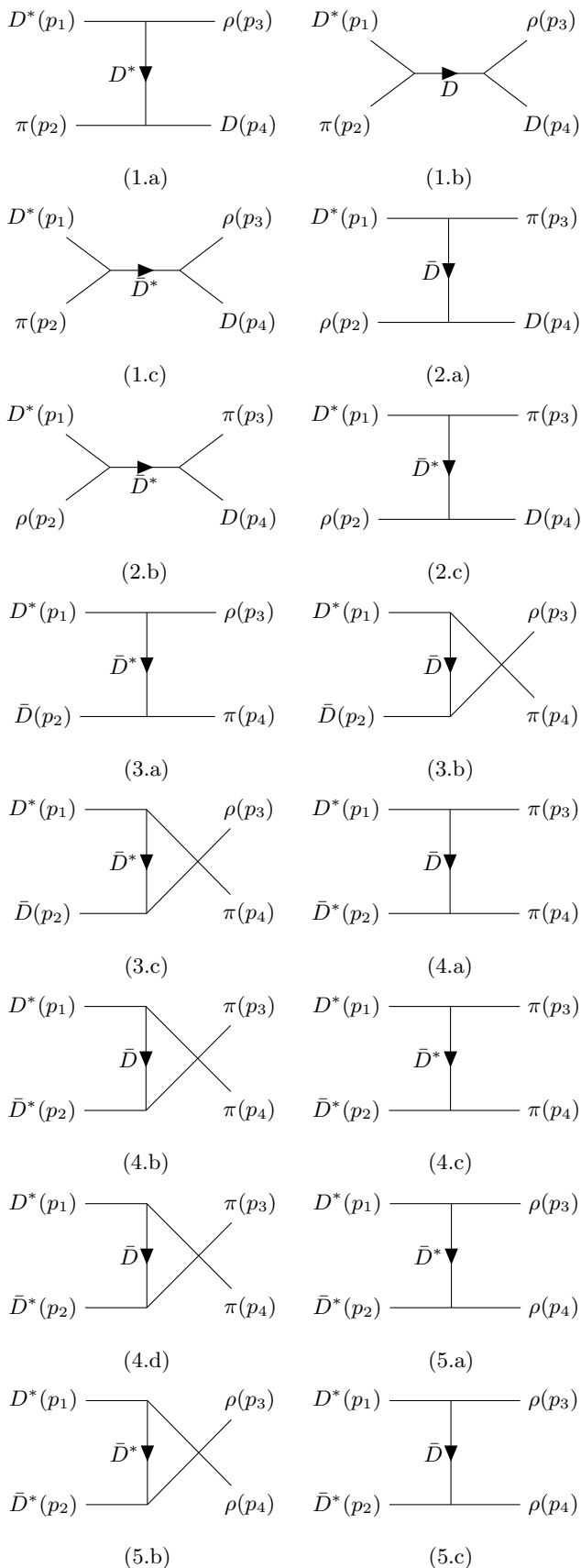


FIG. 1. Diagrams contributing to the processes $D^*\pi \rightarrow \rho D$ [diagrams (1a)-(1c)], $D^*\rho \rightarrow \pi D$ [diagrams (2a)-(2c)], $D^*\bar{D} \rightarrow \rho\pi$ [diagrams (3a)-(3c)], $D^*\bar{D}^* \rightarrow \pi\pi$ [diagrams (4a)-(4d)], $D^*\bar{D}^* \rightarrow \rho\rho$ [diagrams (5a)-(5c)].

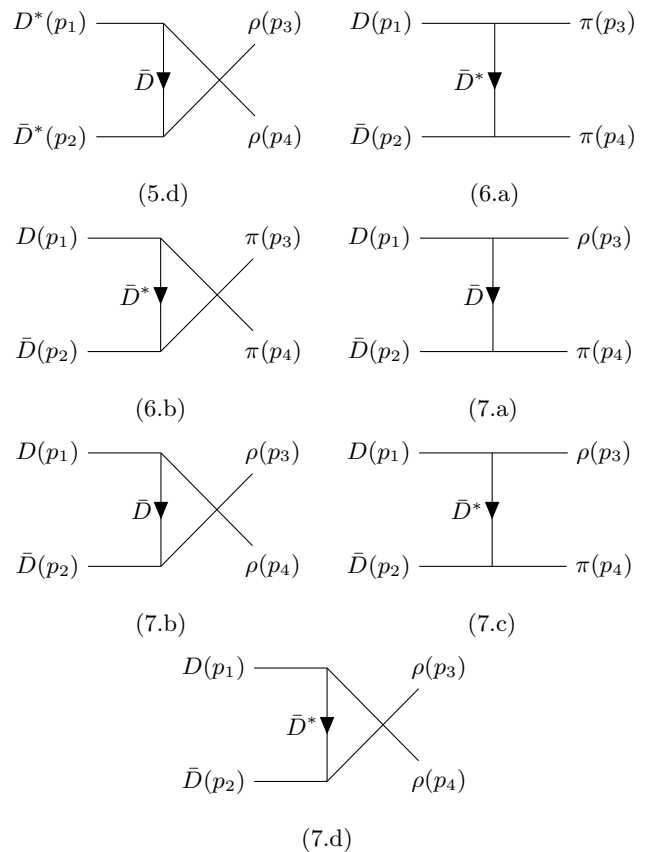


FIG. 2. Diagrams contributing to the processes $D^*\bar{D}^* \rightarrow \rho\rho$ [diagram (5d)], $DD \rightarrow \pi\pi$ [diagrams (6a) and (6b)], and $D\bar{D} \rightarrow \rho\rho$ [diagrams (7a)-(7d)], without specification of the charges of the particles.

where $g_{1i,r} = (2I_{1i,r} + 1)(2I_{2i,r} + 1)$ and $g_{2i,r} = (2S_{1i,r} + 1)(2S_{2i,r} + 1)$ are the degeneracy factors of the particles in the initial state. The cross sections for the inverse processes of those shown in Figs. 1 and 2 can be calculated through the use of the detailed balance relation.

In the evaluation of the cross sections, to prevent the artificial increase of the amplitudes with the energy and take into account the finite size of the hadrons, we introduce form factors in each vertex in the reactions. Fortunately, all the form factors for the vertices $D\pi D^*$, $D\rho D$, $D^*\rho D^*$, $D^*\pi D^*$ and $D\rho D^*$ have already been calculated with the method of QCD sum rules in previous works [18–21]. They were parametrized with the following forms [18]:

$$I) \quad g_{M_1 M_2 M_3} = \frac{A}{Q^2 + B} \quad (5)$$

and

$$II) \quad g_{M_1 M_2 M_3} = A e^{-(Q^2/B)} \quad (6)$$

where M_1 is the off-shell meson in the vertex and Q^2 is its euclidean four momentum squared. The parameters A and B are given in Table I.

M_1	M_2	M_3	Form	A	B
$D\pi D^*$			I	126	11.9
$D\rho D$			I	37.5	12.1
$D^*\rho D^*$			II	4.9	13.3
$D^*\pi D^*$			II	4.8	6.8
$D\rho D^*$			I	234	44

TABLE I. Parameters for the form factors in the $M_1 M_2 M_3$ vertex [18]. The meson M_1 is off-shell.

The final element in this set of reactions is the formation of the D^* meson from the pion and D meson. Adopting a similar approach as in Refs. [6, 10, 22], the scattering cross section for the process $D\pi \rightarrow D^*$ is given by the spin-averaged relativistic Breit-Wigner cross section,

$$\sigma_{D\pi \rightarrow D^*} = \frac{g_{D^*} g_{\bar{D}} 4\pi}{g_{\bar{D}} g_{\pi} p_{cm}^2} \frac{s \Gamma_{D^* \rightarrow D\pi}^2}{(s - m_{D^*}^2)^2 + s \Gamma_{D^* \rightarrow D\pi}^2}, \quad (7)$$

where g_{D^*} , $g_{\bar{D}}$ and g_{π} are the degeneracy of D^* , \bar{D} and π mesons, respectively; p_{cm} is the momentum in CM frame; $\Gamma_{D^* \rightarrow D\pi}$ is the total decay width for the reaction $D^* \rightarrow D\pi$, which is supposed to be effectively \sqrt{s} -dependent via the formula

$$\Gamma_{D^* \rightarrow D\pi}(\sqrt{s}) = \frac{g_{D^* \rightarrow D\pi}^2}{2\pi s} p_{cm}^3(\sqrt{s}), \quad (8)$$

with the value of constant $g_{D^* \rightarrow D\pi}$ being determined from the experimental value of $\Gamma_{D^* \rightarrow D\pi}(\sqrt{s})$.

We have employed in the computations of the present work the isospin-averaged masses: $m_{\pi} = 137.3$ MeV, $m_{\rho} = 775.2$ MeV, $m_D = 1867.2$ MeV, $m_{D^*} = 2008.6$ MeV; and for the decay width: $\Gamma_{D^* \rightarrow D\pi} = 69.2$ keV.

In Fig. 3a the D^* absorption cross sections for the processes summarized in Figs. 1 and 2 are plotted as a function of the CM energy \sqrt{s} . It can be seen that the exothermic processes with only light mesons in the final state have higher magnitudes at smaller energies. Among these, the $D^* \bar{D}^* \rightarrow \pi\pi$ presents a faster decreasing as the energy increases. On the other hand, up to moderate energies the process $D^* \bar{D}^* \rightarrow \rho\rho$ is larger than other reactions, as a consequence of two effective couplings involving three vector mesons [10]. In the case of reactions with a D meson in the final state, the only endothermic process, $D^* \pi \rightarrow \rho D$, has the cross section approximately one order of magnitude higher than that of the reaction $D^* \rho \rightarrow \pi D$ for higher energies. In Fig. 3b, the D absorption cross sections are displayed. The processes with only light mesons in the final state have greater cross sections typically by two or three orders of magnitude.

These results allow to quantitatively estimate and compare the different contributions for the D^* and D absorptions. Also, they have smaller magnitudes when contrasted with the equivalent reactions involving strange mesons reported in Refs. [6, 10, 11].

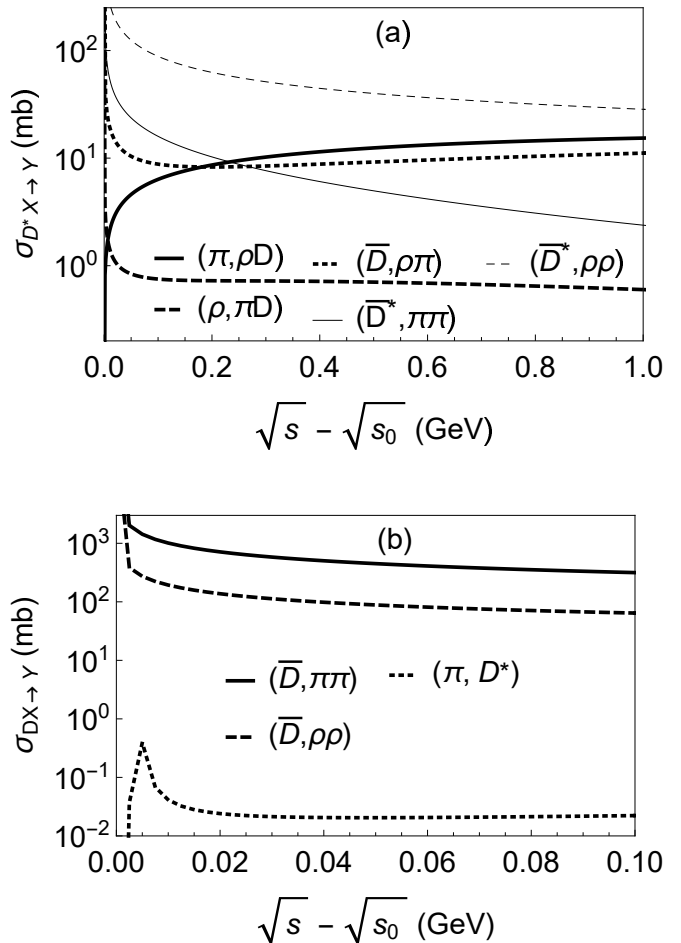


FIG. 3. a) D^* absorption cross sections for processes (1)-(5) shown in Figs. 1 and 2 as a function of the CM energy \sqrt{s} . b) D absorption cross sections for processes (6)-(7) shown in Fig. 2 and for that described in Eq. (7) as a function of the CM energy \sqrt{s} . The label (X, Y) identifies the respective channel $D^{(*)}X \rightarrow Y$ considered.

For the sake of completeness, we also present the cross sections related to the D^* and D production, obtained through the detailed balance relation involving the aforementioned processes. They are shown in Fig. 4 as functions of the CM energy. Except for the case of $\sigma_{\rho D \rightarrow D^* \pi}$, they are all endothermic. The effects encoded in the detailed balance relations produce cross sections with different magnitudes when compared with the results shown in Fig. 3.

To summarize: with a few exceptions, we find cross sections which are mostly in the range $0.01 - 10$ mb, in rough agreement with most of the other existing calculations [23]. The exceptions are the charm annihilation processes $D\bar{D} \rightarrow \pi\pi$, $D\bar{D} \rightarrow \rho\rho$ and $D^* \bar{D}^* \rightarrow \rho\rho$, which are much larger. However, these processes do not contribute much to the rate equation (see below) since their cross sections appear multiplied by the square of the charm density (n_D or $n_{\bar{D}}$), which is a small number.

Having these cross sections, the next step is to compute

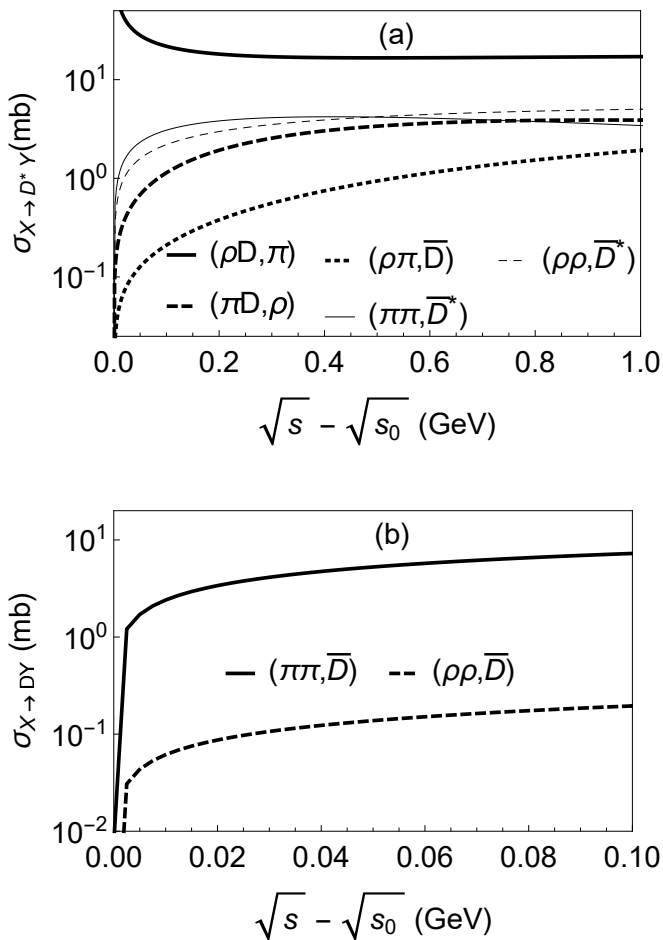


FIG. 4. a) D^* production cross sections for inverse processes (1)-(5) shown in Figs. 1 and 2 as a function of the CM energy \sqrt{s} . b) D production cross sections for inverse processes (6)-(7) shown in Fig. 2 as a function of the CM energy \sqrt{s} . The label (X, Y) identifies the respective channel $X \rightarrow D^{(*)}Y$ considered.

the thermal cross sections.

C. Thermal cross sections

In a relativistic heavy-ion collision the reactions discussed above should occur typically in a later stage, namely in an equilibrated hadron medium at temperatures between 100 and 160 MeV. Then, the relevant dynamical quantity is the cross section calculated in the kinematical regime where the colliding particles have momenta of the order of the temperature. We define the thermally averaged cross section, or simply thermal cross

section, for a given process $ab \rightarrow cd$ as:

$$\begin{aligned} \langle \sigma_{ab \rightarrow cd} v_{ab} \rangle &= \frac{\int d^3 \mathbf{p}_a d^3 \mathbf{p}_b f_a(\mathbf{p}_a) f_b(\mathbf{p}_b) \sigma_{ab \rightarrow cd} v_{ab}}{\int d^3 \mathbf{p}_a d^3 \mathbf{p}_b f_a(\mathbf{p}_a) f_b(\mathbf{p}_b)} \\ &= \frac{1}{4 \beta_a^2 K_2(\beta_a) \beta_b^2 K_2(\beta_b)} \\ &\quad \times \int_{z_0}^{\infty} dz K_1(z) \sigma(s = z^2 T^2) \\ &\quad \times [z^2 - (\beta_a + \beta_b)^2] [z^2 - (\beta_a - \beta_b)^2], \end{aligned} \quad (9)$$

where v_{ab} is the relative velocity between the two initial interacting particles a and b , the function $f_i(\mathbf{p}_i)$ is the temperature T -dependent Bose-Einstein distribution of particles of species i , $\beta_i = m_i/T$, $z_0 = \max(\beta_a + \beta_b, \beta_c + \beta_d)$, and K_1 and K_2 the modified Bessel functions of second kind.

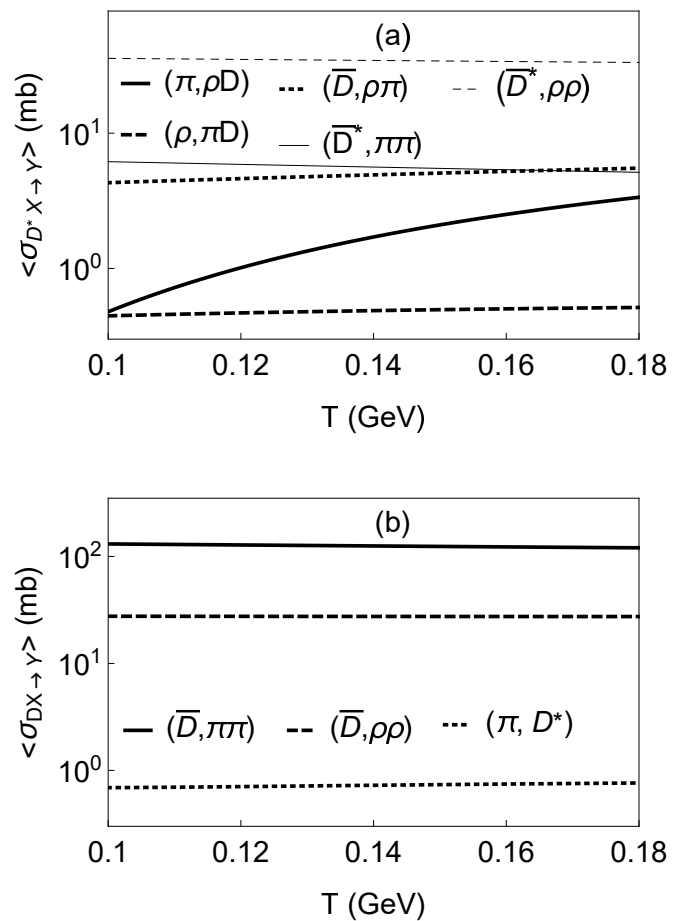


FIG. 5. a) Thermal cross sections as a function of the temperature for the D^* absorption via processes (1)-(5) shown in Figs. 1 and 2. b) Same as a) but for the D absorption via processes (6)-(7) shown in Fig. 2 and for that described in Eq. (7). The label (X, Y) identifies the respective channel $D^{(*)}X \rightarrow Y$ considered.

In Figs. 5 and 6 we plot the thermal cross sections as a function of the temperature for the D^* and D meson

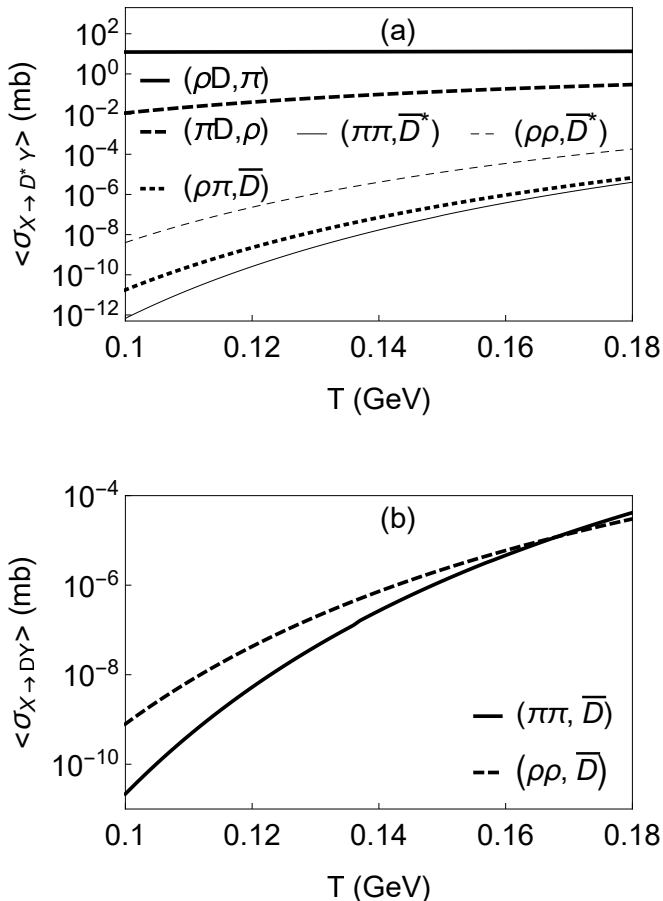


FIG. 6. a) Thermal cross sections as a function of the temperature for the D^* production via inverse processes to those shown in Figs. 1 and 2. b) Same as a) but for the D production via inverse processes to those shown in Fig. 2. The label (X, Y) identifies the respective channel $X \rightarrow D^{(*)}Y$ considered.

absorption via processes (1)-(7) shown in Figs. 1 and 2. For the sake of comparison, the thermal cross sections for the respective inverse reactions are also plotted. Within the considered range of temperatures, it can be seen that the reaction $\rho D \rightarrow D^* \pi$ is the only D^* production reaction with larger cross section than the corresponding inverse reaction. In general, the thermal D^* dissociation cross sections are bigger than those for the production reactions. Also, we notice that the D^* meson absorption is easier by charmed mesons than by light mesons. More specifically, the process $D^* \bar{D}^* \rightarrow \rho \rho$ has the largest thermal cross section, being higher than the D^* meson absorption by π, ρ mesons by one or two orders of magnitude. Interestingly, the $D^{(*)}$ production reactions from light mesons are several orders of magnitude smaller than the corresponding dissociation processes, reflecting the higher energy threshold of these processes.

To conclude this section, we highlight the differences among the magnitudes of thermal cross sections for $D^{(*)}$ dissociation and production reactions, which in principle might play an important role in the time evolution of the D^* multiplicity.

III. EVOLUTION EQUATIONS

Now we move to the analysis of the time evolution of the D^* and D multiplicities during the hadronic stage of heavy ion collisions. To this end, the thermal cross sections estimated in the previous section will be used as input in the momentum-integrated evolution equations for the D^* and D abundances to estimate the gain and loss terms due to $D^{(*)}$ production and absorption. As in the previous works [6, 10], these equations with all considered creation and annihilation reactions are given by:

$$\begin{aligned}
\frac{dN_{D^*}}{d\tau} &= \langle \sigma_{D\rho \rightarrow D^* \pi} v_{D\rho} \rangle n_\rho(\tau) N_D(\tau) - \langle \sigma_{D^* \pi \rightarrow D\rho} v_{D^* \pi} \rangle n_\pi(\tau) N_{D^*}(\tau) + \langle \sigma_{D\pi \rightarrow D^* \rho} v_{D\pi} \rangle n_\pi(\tau) N_D(\tau) \\
&\quad - \langle \sigma_{D^* \rho \rightarrow D\pi} v_{D^* \rho} \rangle n_\rho(\tau) N_{D^*}(\tau) + \langle \sigma_{\pi\rho \rightarrow D^* \bar{D}} v_{\pi\rho} \rangle n_\pi(\tau) N_\rho(\tau) - \langle \sigma_{D^* \bar{D} \rightarrow \rho\pi} v_{D^* \bar{D}} \rangle n_{\bar{D}}(\tau) N_{D^*}(\tau) \\
&\quad + \langle \sigma_{\pi\pi \rightarrow D^* \bar{D}^*} v_{\pi\pi} \rangle n_\pi(\tau) N_\pi(\tau) - \langle \sigma_{D^* \bar{D}^* \rightarrow \pi\pi} v_{D^* \bar{D}^*} \rangle n_{\bar{D}^*}(\tau) N_{D^*}(\tau) + \langle \sigma_{\rho\rho \rightarrow D^* \bar{D}^*} v_{\rho\rho} \rangle n_\rho(\tau) N_\rho(\tau) \\
&\quad - \langle \sigma_{D^* \bar{D}^* \rightarrow \rho\rho} v_{D^* \bar{D}^*} \rangle n_{\bar{D}^*}(\tau) N_{D^*}(\tau) + \langle \sigma_{D\pi \rightarrow D^*} v_{D\pi} \rangle n_\pi(\tau) N_D(\tau) - \langle \Gamma_{D^*} \rangle N_{D^*}(\tau), \\
\frac{dN_D}{d\tau} &= \langle \sigma_{\pi\pi \rightarrow D\bar{D}} v_{\pi\pi} \rangle n_\pi(\tau) N_\pi(\tau) - \langle \sigma_{D\bar{D} \rightarrow \pi\pi} v_{D\bar{D}} \rangle n_{\bar{D}}(\tau) N_D(\tau) + \langle \sigma_{\rho\rho \rightarrow D\bar{D}} v_{\rho\rho} \rangle n_\rho(\tau) N_\rho(\tau) \\
&\quad - \langle \sigma_{D\bar{D} \rightarrow \rho\rho} v_{D\bar{D}} \rangle n_{\bar{D}}(\tau) N_D(\tau) + \langle \sigma_{D^* \pi \rightarrow D\rho} v_{D^* \pi} \rangle n_\pi(\tau) N_{D^*}(\tau) - \langle \sigma_{D\rho \rightarrow D^* \pi} v_{D\rho} \rangle n_\rho(\tau) N_D(\tau) \\
&\quad + \langle \sigma_{D^* \rho \rightarrow D\pi} v_{D^* \rho} \rangle n_\rho(\tau) N_{D^*}(\tau) - \langle \sigma_{D\pi \rightarrow D^* \rho} v_{D\pi} \rangle n_\pi(\tau) N_D(\tau) + \langle \sigma_{\pi\rho \rightarrow D^* \bar{D}} v_{\pi\rho} \rangle n_\pi(\tau) N_\rho(\tau) \\
&\quad - \langle \sigma_{D^* \bar{D} \rightarrow \rho\pi} v_{D^* \bar{D}} \rangle n_{\bar{D}}(\tau) N_{D^*}(\tau) + \langle \Gamma_{D^*} \rangle N_{D^*}(\tau) - \langle \sigma_{D\pi \rightarrow D^*} v_{D\pi} \rangle n_\pi(\tau) N_D(\tau). \tag{10}
\end{aligned}$$

where $n_i(\tau)$ are $N_i(\tau)$ denote the density and the abundances of the involved mesons at proper time τ .

The rate equations above and their gain and loss contributions deserve some comments. The decay of D^*

and its regeneration from the daughter particles D and π are included in the last line of the two evolution equations. However, due to the small value of the D^* decay width Γ_{D^*} , the lifetime of the D^* mesons is much greater than that of the hadron gas presumed in this work (of the order of 10 fm/c). Therefore, the decay of D^* can be neglected in the rate equation. Moreover, as in Refs. [6, 10, 11], some terms yield very small contributions because of the smallness of their thermal cross sections and/or small values of $D^{(*)}$ densities with respect to the ones of light mesons, which are the most abundant particles in a hadron gas. Then, several terms associated to the processes with two charmed mesons in initial or final states can be safely neglected.

To obtain the solutions of Eq. (10) we assume that the pions, rho and charm mesons in the reactions contributing to the D^* and D multiplicities are in thermal equilibrium. Then, the density $n_i(\tau)$ is written as [14, 15, 22, 24–26]

$$n_i(\tau) \approx \frac{1}{2\pi^2} \gamma_i g_i m_i^2 T(\tau) K_2 \left(\frac{m_i}{T(\tau)} \right), \quad (11)$$

where γ_i and g_i are the fugacity factor and the degeneracy factor of the particle of type i , respectively. We obtain the multiplicity $N_i(\tau)$ multiplying the density $n_i(\tau)$ by the volume $V(\tau)$. To model the dynamics of relativistic heavy ion collisions in the hadronic phase, the temperature $T(\tau)$ and volume $V(\tau)$ are parametrized according to the boost invariant Bjorken picture with an accelerated transverse expansion [15, 22, 24, 25]. The τ dependence of $V(\tau)$ and T are thus given by

$$T(\tau) = T_C - (T_H - T_F) \left(\frac{\tau - \tau_H}{\tau_F - \tau_H} \right)^{\frac{4}{5}},$$

$$V(\tau) = \pi \left[R_C + v_C (\tau - \tau_C) + \frac{a_C}{2} (\tau - \tau_C)^2 \right]^2 \tau c, \quad (12)$$

where R_C and τ_C denote the final transverse and longitudinal sizes of the QGP; v_C and a_C are its transverse flow velocity and transverse acceleration at τ_C ; T_C is the critical temperature of the quark-hadron transition; T_H is the temperature of the hadronic matter at the end of the mixed phase, occurring at the time τ_H ; and the kinetic freeze-out temperature T_F leads to a freeze-out time τ_F . We notice that this simple picture of the hydrodynamic evolution of fluid should be seen as a tool to mimic the essential features of hydrodynamic expansion and cooling of the hadron gas. The collisions chosen for this study are the central $Pb - Pb$ collisions at $\sqrt{s_{NN}} = 5$ TeV at the LHC. In this way, we use the parameter choice of Ref. [25], which, for convenience, is summarized in Table II.

We assume that the total number of charm quarks (N_c) in charmed hadrons remains approximately conserved

TABLE II. Parameters used in Eq. (12) for central $Pb - Pb$ collisions at $\sqrt{s_{NN}} = 5$ TeV [25].

v_C (c)	a_C (c ² /fm)	R_C (fm)
0.5	0.09	11
τ_C (fm/c)	τ_H (fm/c)	τ_F (fm/c)
7.1	10.2	21.5
T_C (MeV)	T_H (MeV)	T_F (MeV)
156	156	115
N_c	$N_\pi(\tau_F)$	$N_\rho(\tau_F)$
14	2410	179
$N_D(\tau_H)$	$N_{D^*}(\tau_H)$	
4.7	6.3	

during the fireball evolution, i.e. $n_c(\tau) \times V(\tau) = N_c$. Then we use a time-dependent charm quark fugacity factor γ_c in Eq. (11) to calculate the charmed mesons in order to keep N_c constant. Besides, the total number of pions and ρ mesons at freeze-out was taken from Refs. [15, 22]. These numbers are displayed in Table II.

The time evolution of the D and D^* abundances is plotted in Fig. 7 as a function of the proper time. These results suggest that the interactions of the D 's and D^* with the hadronic medium through the reactions discussed previously in HICs produce only small changes in the multiplicities: while N_{D^*} grows 5%, N_D decreases by 7%. In the figure we also show the ratio $R = D^*/D$. This is the main result of our work. We conclude that the information contained in open charm multiplicities will be propagated from the hadronization time to the kinetic freeze-out time without much distortion.

Finally, in order to make predictions which can be confronted with experimental data we compute the ratio R as a function of the multiplicity density of charged particles measured at midrapidity, i.e. $\mathcal{N} = [dN_{ch}/d\eta(\eta < 0.5)]^{1/3}$. The quantity \mathcal{N} is usually considered a measure of the size of the system [27, 28], which in turn is directly related to the kinetic freeze-out temperature [29]. An empirical connection between these variables was established in Ref. [6]. Assuming that the hadron gas suffers a Bjorken-like cooling, the freeze-out time τ_f is related to the freeze-out temperature T_f through the expression:

$$\tau_f = \tau_h \left(\frac{T_H}{T_F} \right)^3. \quad (13)$$

Next, we use the empirical relation between T_F and \mathcal{N} extracted from [29] and parametrized as [6]:

$$T_F = T_{F0} e^{-b\mathcal{N}}, \quad (14)$$

where $T_{F0} = 132.5$ MeV and $b = 0.02$. Then, inserting (14) into (13) we obtain

$$\tau_F \propto e^{3b\mathcal{N}}. \quad (15)$$

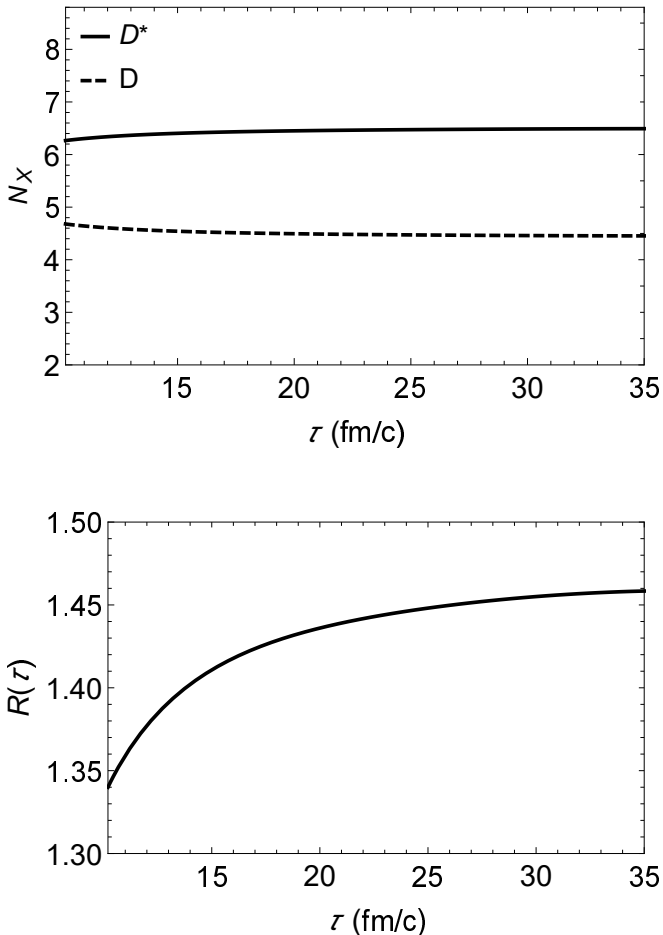


FIG. 7. Upper panel: D and D^* abundances as a function of the proper time τ in central $Pb - Pb$ collisions at $\sqrt{s_{NN}} = 5$ TeV, calculated with the parameters from Table II. Lower panel: evolution of the ratio $R = D^*/D$.

Thus, \mathcal{N} provides an estimate of the duration of the hadronic phase. Larger systems have bigger \mathcal{N} and live longer. We use Eq. (15) in the solutions of Eq. (10) to determine R as a function \mathcal{N} .

In Fig. 8 we show the D^* and D abundances and the ratio $R = D^*/D$ as a function of \mathcal{N} . As it can be seen in the upper panel of the figure, the abundances depend strongly on the system size. However, the ratio D^*/D does not change significantly. This fact contrasts with the case of the strange K^* and K mesons discussed in Ref. [6], where the longer the hadronic system lasts, the smaller is the ratio K^*/K . This difference can be attributed to the difference in the decay widths $D^* \rightarrow D \pi$ and $K^* \rightarrow K \pi$, with the latter being much larger.

To the best of our knowledge, there are so far no data available to perform a direct comparison with the predictions presented in Fig. 8.

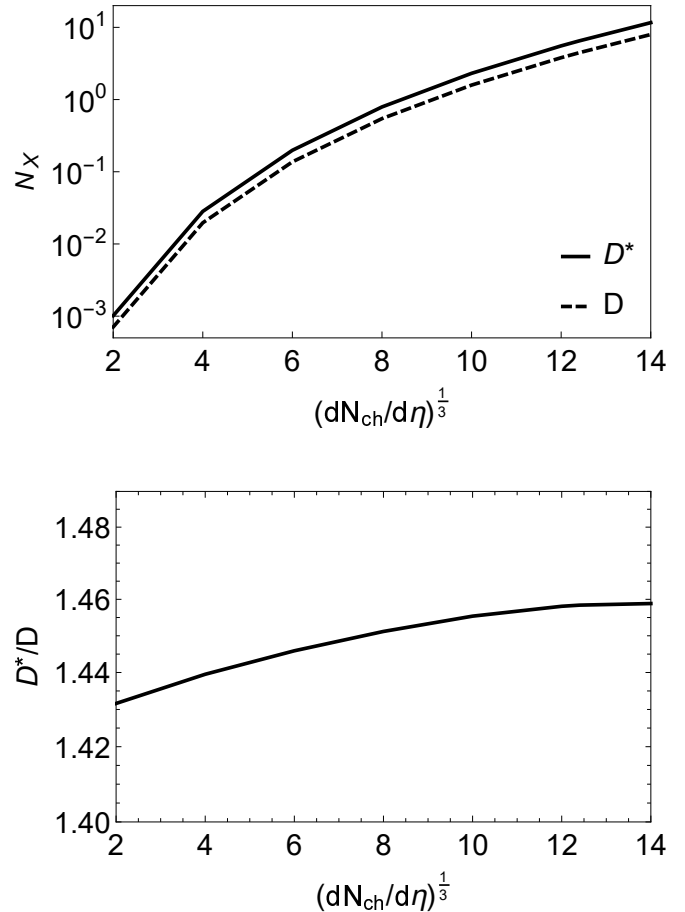


FIG. 8. Upper panel: D and D^* abundances as a function of \mathcal{N} . Lower panel: D^*/D with initial condition $D^*/D = 1.34$ as a function of \mathcal{N} .

IV. CONCLUDING REMARKS

In this work we have performed a systematic analysis of the $D^{(*)}$ meson dissociation in the hadron gas phase of heavy ion collisions. Using an effective Lagrangian formalism, we have evaluated the thermal production and absorption cross sections of the D^* and D mesons in a hadron gas. The couplings and form factors in all the vertices were previously computed with QCD sum rules. Therefore, in our case, much of the uncertainties and arbitrariness, inherent to this kind of calculation, were avoided.

The obtained cross sections were used as input in the rate equations to estimate the time evolution of the $D^{(*)}$ multiplicities and the ratio D^*/D during the hadron gas phase of heavy ion collisions. The multiplicities of D and D^* remain almost constant during the evolution of the hadron gas. The ratio D^*/D suffers only a slight increase. This result indicates that charm is already in chemical equilibrium at the beginning of the hadron gas phase. Therefore our calculation can be regarded as a microscopic justification of the use of the statistical hadroniza-

tion model to compute the charm meson abundances.

The lifetime of a hadronic fireball is, of course, not directly measurable and we would like to make contact with experimental data. To this end, we have assumed a Bjorken type cooling for the hadron gas and used an empirical relation between the freeze-out temperature and the multiplicity density of charged particles at midrapidity. With this procedure we estimated the ratio D^*/D as a function of $(dN/d\eta(\eta = 0))$. As expected from the first part of the calculation, we found that D^*/D slightly increases if the hadronic medium lives longer, in sharp contrast to the K^*/K ratio, computed in [6] with the same methods.

We believe that these results can be compared with future experimental data, and may contribute to a better understanding of the hadron medium created in heavy ion collisions.

ACKNOWLEDGMENTS

The authors would like to thank the Brazilian funding agencies for their financial support: CNPq (LMA: contracts 309950/2020-1 and 400546/2016-7), FAPESB (LMA: contract INT0007/2016) and the INCT-FNA.

Appendix A: Amplitudes

Here we give the explicit expressions for the contributions to the amplitudes in Eq. (2), associated to the processes shown in Figs. 1 and. 2. They are [6, 10, 11]

$$\begin{aligned} \mathcal{M}_{(1a)} &= \tau_{rs}^{(i)} \tau_{r's'}^{(j)} g_{\pi DD^*} g_{\rho D^* D^*} \epsilon_1^{\alpha* \beta} \frac{1}{t - m_{D^*}^2 + im_{D^*} \Gamma_{D^*}} \left(-g^{\mu\nu} + \frac{(p_1 - p_3)^\mu (p_1 - p_3)^\nu}{m_{D^*}^2} \right) (p_2 + p_4)_\mu \\ &\quad \times \left((2p_1 - p_3)_{\beta g_{\alpha\nu}} - (p_1 + p_3)_{\nu g_{\alpha\beta}} - (p_1 - 2p_3)_{\alpha g_{\beta\nu}} \right), \\ \mathcal{M}_{(1b)} &= -\tau_{rs}^{(i)} \tau_{r's'}^{(j)} g_{\pi DD^*} g_{\rho DD^*} \epsilon_1^{\mu* \nu} \frac{1}{s - m_D^2} (p_1 + 2p_2)_\mu (p_3 + 2p_4)_\nu, \\ \mathcal{M}^{(1.c)} &= g_{\rho DD^*} g_{\pi D^* D^*} \epsilon_1^\mu \epsilon_3^\nu \epsilon_{\mu\gamma\delta\alpha} \epsilon_{\nu\sigma\rho\beta} \frac{1}{s - m_{D^*}^2 + im_{D^*} \Gamma_{D^*}} \left(-g^{\alpha\beta} + \frac{(p_1 + p_2)^\alpha (p_1 + p_2)^\beta}{m_{D^*}^2} \right) p_1^\gamma p_2^\delta p_3^\sigma p_4^\rho, \end{aligned} \quad (\text{A1})$$

$$\begin{aligned} \mathcal{M}_{(2a)} &= -\tau_{rs}^{(i)} \tau_{r's'}^{(j)} g_{\pi DD^*} g_{\rho DD^*} \epsilon_1^\mu \epsilon_2^\nu \frac{1}{t - m_D^2} (p_1 - 2p_3)_\mu (2p_4 - p_2)_\nu, \\ \mathcal{M}_{(2b)} &= -\tau_{rs}^{(i)} \tau_{r's'}^{(j)} g_{\pi DD^*} g_{\rho D^* D^*} \epsilon_1^{\alpha\beta} \frac{1}{s - m_{D^*}^2 + im_{D^*} \Gamma_{D^*}} \left(-g^{\mu\nu} + \frac{(p_1 + p_2)^\mu (p_1 + p_2)^\nu}{m_{D^*}^2} \right) (p_3 - p_4)_\mu \\ &\quad \times \left((2p_1 + p_2)_{\beta g_{\alpha\nu}} - (p_1 - p_2)_{\nu g_{\alpha\beta}} - (p_1 + 2p_2)_{\alpha g_{\beta\nu}} \right) \\ \mathcal{M}^{(2.c)} &= g_{\rho DD^*} g_{\pi D^* D^*} \epsilon_1^\mu \epsilon_2^\nu \epsilon_{\mu\gamma\delta\alpha} \epsilon_{\nu\sigma\rho\beta} \frac{1}{t - m_{D^*}^2 + im_{D^*} \Gamma_{D^*}} \left(-g^{\alpha\beta} + \frac{(p_1 - p_3)^\alpha (p_1 - p_3)^\beta}{m_{D^*}^2} \right) p_1^\gamma p_2^\delta p_3^\sigma p_4^\rho, \end{aligned} \quad (\text{A2})$$

$$\begin{aligned} \mathcal{M}_{(3a)} &= \tau_{rs}^{(i)} \tau_{r's'}^{(j)} g_{\pi DD^*} g_{\rho D^* D^*} \epsilon_1^{\alpha* \beta} \frac{1}{t - m_{D^*}^2 + im_{D^*} \Gamma_{D^*}} \left(-g^{\mu\nu} + \frac{(p_1 - p_3)^\mu (p_1 - p_3)^\nu}{m_{D^*}^2} \right) (p_2 + p_4)_\mu \\ &\quad \times \left((2p_3 - p_1)_{\alpha g_{\beta\nu}} - (p_1 + p_3)_{\nu g_{\alpha\beta}} + (2p_1 - p_3)_{\beta g_{\alpha\nu}} \right), \\ \mathcal{M}_{(3b)} &= \tau_{rs}^{(i)} \tau_{r's'}^{(j)} g_{\pi DD^*} g_{\rho DD^*} \epsilon_1^{\mu* \nu} \frac{1}{u - m_D^2} (2p_4 - p_1)_\mu (2p_2 - p_3)_\nu, \\ \mathcal{M}^{(3.c)} &= g_{\pi D^* D^*} g_{\rho DD^*} \epsilon_1^\mu \epsilon_3^\nu \epsilon_{\mu\gamma\delta\beta} \epsilon_{\nu\sigma\rho\alpha} \frac{1}{u - m_{D^*}^2 + im_{D^*} \Gamma_{D^*}} \left(-g^{\alpha\beta} + \frac{(p_1 - p_4)^\alpha (p_1 - p_4)^\beta}{m - D^{*2}} \right) p_1^\gamma p_4^\delta p_2^\sigma p_3^\rho, \end{aligned} \quad (\text{A3})$$

$$\begin{aligned} \mathcal{M}_{(4a)} &= \tau_{rs}^{(i)} \tau_{r's'}^{(j)} g_{\pi DD^*}^2 \epsilon_1^\mu \epsilon_2^\nu \frac{1}{t - m_D^2} (p_1 - p_3)_\mu (p_2 - 2p_4)_\nu, \\ \mathcal{M}_{(4b)} &= \tau_{rs}^{(i)} \tau_{r's'}^{(j)} g_{\pi DD^*}^2 \epsilon_1^\mu \epsilon_2^\nu \frac{1}{u - m_D^2} (2p_1 - 2p_4)_\mu (p_2 - 2p_3)_\nu \\ \mathcal{M}^{(4.c)} &= g_{\pi D^* D^*}^2 \epsilon_1^\mu \epsilon_2^\nu \epsilon_{\mu\gamma\delta\alpha} \epsilon_{\nu\sigma\rho\beta} \frac{1}{t - m_{D^*}^2 + im_{D^*} \Gamma_{D^*}} \left(-g^{\alpha\beta} + \frac{(p_1 - p_3)^\alpha (p_1 - p_3)^\beta}{m_{D^*}^2} \right) p_1^\gamma p_3^\delta p_2^\sigma p_4^\rho, \\ \mathcal{M}^{(4.d)} &= -g_{\pi D^* D^*}^2 \epsilon_1^\mu \epsilon_2^\nu \epsilon_{\mu\gamma\delta\alpha} \epsilon_{\nu\sigma\rho\beta} \frac{1}{u - m_{D^*}^2 + im_{D^*} \Gamma_{D^*}} \left(-g^{\alpha\beta} + \frac{(p_1 - p_4)^\alpha (p_1 - p_4)^\beta}{m_{D^*}^2} \right) p_1^\delta p_4^\gamma p_2^\sigma p_3^\rho, \end{aligned} \quad (\text{A4})$$

$$\begin{aligned}
\mathcal{M}_{(5a)} &= \tau_{rs}^{(i)} \tau_{r's'}^{(j)} g_{\rho D^* D^*}^2 \epsilon_1^\alpha \epsilon_3^{*\beta} \epsilon_2^\gamma \epsilon_4^{*\delta} \frac{1}{t - m_{D^*}^2 + im_{D^*} \Gamma_{D^*}} \left(-g^{\mu\nu} + \frac{(p_1 - p_3)^\mu (p_1 - p_3)^\nu}{m_{D^*}^2} \right) \\
&\quad \times \left((2p_3 - p_1)_{\alpha g \beta \mu} - (p_1 + p_3)_{\mu g \alpha \beta} + (2p_1 - p_3)_{\beta g \alpha \nu} \right) \left((p_2 + p_4)_{\gamma g \delta \nu} + (p_2 - 2p_4)_{\nu g \gamma \nu} \right), \\
\mathcal{M}_{(5b)} &= \tau_{rs}^{(i)} \tau_{r's'}^{(j)} g_{\rho D^* D^*}^2 \epsilon_1^\alpha \epsilon_4^{*\beta} \epsilon_2^\gamma \epsilon_3^{*\delta} \frac{1}{u - m_{D^*}^2 + im_{D^*} \Delta_{D^*}} \left(-g^{\mu\nu} + \frac{(p_1 - p_4)^\mu (p_1 - p_4)^\nu}{m_{D^*}^2} \right) \\
&\quad \times \left((2p_4 - p_1)_{\alpha g \beta \mu} - (p_1 + p_4)_{\mu g \alpha \beta} + (2p_1 - p_4)_{\beta g \alpha \nu} \right) \left((p_2 + p_3)_{\gamma g \nu} + (p_2 - 2p_3)_{\nu g \gamma \nu} + (p_3 - 2p_2)_{\delta g \gamma \nu} \right), \\
\mathcal{M}^{(5.c)} &= -g_{\rho D D^*}^2 \epsilon_1^\alpha \epsilon_3^{*\beta} \epsilon_2^\gamma \epsilon_4^{*\delta} \epsilon_{\alpha\beta\mu\nu} \epsilon_{\gamma\delta\sigma\omega} \frac{1}{t - m_D^2} p_1^\nu p_3^\mu p_2^\sigma p_4^\omega, \\
\mathcal{M}^{(5.d)} &= g_{\rho D D^*}^2 \epsilon_1^\alpha \epsilon_3^{*\beta} \epsilon_2^\gamma \epsilon_4^{*\delta} \epsilon_{\alpha\delta\mu\nu} \epsilon_{\gamma\beta\sigma\omega} \frac{1}{u - m_D^2} p_1^\mu p_4^\nu p_2^\sigma p_3^\omega,
\end{aligned}$$

$$\begin{aligned}
\mathcal{M}_{(6a)} &= \tau_{rs}^{(i)} \tau_{r's'}^{(j)} g_{\pi D D^*}^2 \frac{1}{t - m_{D^*}^2 + im_{D^*} \Gamma_{D^*}} \left(-g^{\mu\nu} + \frac{(p_1 - p_3)^\mu (p_1 - p_3)^\nu}{m_{D^*}^2} \right) (p_1 + p_3)_\mu (p_2 + p_4)_\nu, \\
\mathcal{M}_{(6b)} &= \tau_{rs}^{(i)} \tau_{r's'}^{(j)} g_{\pi D D^*}^2 \frac{1}{u - m_{D^*}^2 + im_{D^*} \Gamma_{D^*}} \left(-g^{\mu\nu} + \frac{(p_1 - p_4)^\mu (p_1 - p_4)^\nu}{m_{D^*}^2} \right) (p_1 + p_4)_\mu (p_2 + p_3)_\nu, \quad (\text{A5})
\end{aligned}$$

$$\begin{aligned}
\mathcal{M}_{(7a)} &= \tau_{rs}^{(i)} \tau_{r's'}^{(j)} g_{\rho D^* D^*}^2 \epsilon_3^{*\mu} \epsilon_4^{*\nu} \frac{1}{t - m_D^2} (2p_1 - p_3)_\mu (2p_2 - p_4)_\nu, \\
\mathcal{M}_{(7b)} &= \tau_{rs}^{(i)} \tau_{r's'}^{(j)} g_{\rho D^* D^*}^2 \epsilon_4^{*\mu} \epsilon_3^{*\nu} \frac{1}{t - m_D^2} (2p_1 - p_4)_\mu (2p_2 - p_3)_\nu, \\
\mathcal{M}^{(7.c)} &= g_{\rho D D^*}^2 \epsilon_3^\alpha \epsilon_4^\beta \epsilon_{\mu\gamma\delta\alpha} \epsilon_{\nu\sigma\rho\beta} \frac{1}{t - m_{D^*}^2 + im_{D^*} \Gamma_{D^*}} \left(-g^{\mu\nu} + \frac{(p_1 - p_3)^\mu (p_1 - p_3)^\nu}{m_{D^*}^2} \right) p_1^\delta p_3^\gamma p_2^\rho p_4^\sigma, \\
\mathcal{M}^{(7.d)} &= -g_{\rho D D^*}^2 \epsilon_3^\alpha \epsilon_4^\beta \epsilon_{\mu\gamma\delta\alpha} \epsilon_{\nu\sigma\rho\beta} \frac{1}{u - m_{D^*}^2 + im_{D^*} \Gamma_{D^*}} \left(-g^{\mu\nu} + \frac{(p_1 - p_4)^\mu (p_1 - p_4)^\nu}{m_{D^*}^2} \right) p_1^\gamma p_4^\delta p_2^\rho p_3^\sigma, \quad (\text{A6})
\end{aligned}$$

where $\tau_{rs}^{(i,j)}$ is the isospin factor related to i, j -th component of π, ρ isospin triplets and $r(s)$ -th component of D^* isospin doublets; p_1 and p_2 are the momenta of initial state particles, while p_3 and p_4 are those of fi-

nal state particles; s, t, u are the Mandelstam variables: $s = (p_1 + p_2)^2, t = (p_1 - p_3)^2$, and $u = (p_1 - p_4)^2$; and $\epsilon_m^{(*)} \equiv \epsilon^{(*)}(p_m)$ is the polarization vector.

-
- [1] J. Adams *et al.* [STAR], Nucl. Phys. A **757**, 102 (2005).
[2] E. Shuryak, Prog. Part. Nucl. Phys. **62**, 48 (2009).
[3] R. Rapp, D. Blaschke, and P. Crochet, Prog. Part. Nucl. Phys. **65**, 209 (2010).
[4] P. Braun-Munzinger, V. Koch, T. Schafer, and J. Stachel, Phys. Rep. **621**, 76 (2016).
[5] F. Prino and R. Rapp, J. Phys. G **43**, 093002 (2016).
[6] C. Le Roux, F. S. Navarra and L. M. Abreu, Phys. Lett. B **817**, 136284 (2021).
[7] A. Andronic, P. Braun-Munzinger, M. K. Köhler, A. Mazeliauskas, K. Redlich, J. Stachel and V. Vislavicius, JHEP **07**, 035 (2021) and references therein.
[8] S. Acharya *et al.* [ALICE], JHEP **01**, 174 (2022).
[9] S. Acharya *et al.* [ALICE], Phys. Lett. B **802**, 135225 (2020).
[10] S. Cho and S. H. Lee, Phys. Rev. C **97**, 034908 (2018).
[11] A. Martinez Torres, K. P. Khemchandani, L. M. Abreu, F. S. Navarra and M. Nielsen, Phys. Rev. D **97**, 056001 (2018).
[12] Y. S. Oh, T. Song, and S. H. Lee, Phys. Rev. C **63**, 034901 (2001).
[13] F. Carvalho, F. O. Duraes, F. S. Navarra and M. Nielsen, Phys. Rev. C **72**, 024902 (2005).
[14] L. W. Chen, C. M. Ko, W. Liu and M. Nielsen, Phys. Rev. C **76** (2007), 014906.
[15] S. Cho and S. H. Lee, Phys. Rev. C **88**, 054901 (2013).
[16] A. Martinez Torres, K. P. Khemchandani, F. S. Navarra, M. Nielsen, and L. M. Abreu, Phys. Rev. D **90**, 114023 (2014); **93**, 059902(E) (2016).
[17] L. M. Abreu, K. P. Khemchandani, A. Martinez Torres, F. S. Navarra, and M. Nielsen, Phys. Lett. B **761**, 303 (2016).
[18] M.E. Bracco, M. Chiapparini, F.S. Navarra and M. Nielsen, Prog. Part. Nucl. Phys. **67**, 1019 (2012).
[19] M. E. Bracco, M. Chiapparini, F. S. Navarra and M. Nielsen, Phys. Lett. B **659**, 559 (2008).
[20] B. Osorio Rodrigues, M. E. Bracco, M. Nielsen and F. S. Navarra, Nucl. Phys. A **852**, 127 (2011).
[21] L. M. Abreu, H. P. L. Vieira and F. S. Navarra, Phys. Rev. D **105**, 116029 (2022).

- [22] L. M. Abreu, Phys. Rev. D **103**, 036013 (2021).
- [23] M. He, R. J. Fries and R. Rapp, Phys. Lett. B **701**, 445 (2011); S. Ghosh, S. K. Das, S. Sarkar and J. e. Alam, Phys. Rev. D **84**, 011503 (2011); L. Tolos and J. M. Torres-Rincon, Phys. Rev. D **88**, 074019 (2013); V. Ozvenchuk, J. M. Torres-Rincon, P. B. Gossiaux, L. Tolos and J. Aichelin, Phys. Rev. C **90**, 054909 (2014).
- [24] L. M. Abreu, F. S. Navarra and M. Nielsen, Phys. Rev. C **101**, 014906 (2020).
- [25] S. Cho *et al.* [ExHIC Collaboration], Phys. Rev. C **84**, 064910 (2011); Prog. Part. Nucl. Phys. **95**, 279 (2017).
- [26] P. Koch, B. Muller and J. Rafelski, Phys. Rep. **142**, 167 (1986).
- [27] K. Aamodt *et al.* [ALICE], Phys. Lett. B **696**, 328 (2011).
- [28] M. A. Lisa, S. Pratt, R. Soltz and U. Wiedemann, Ann. Rev. Nucl. Part. Sci. **55**, 357 (2005).
- [29] B. Abelev *et al.* [ALICE Collaboration], Phys. Rev. C **88**, 044910 (2013).